Rev. Adv. Mater. Sci. 50 (2017) 24-30

DEFORMATION AND FRACTURE PROCESSES IN PRE-CRACKED GRAPHENE

A.S. Kochnev[1,2], I.A. Ovid'ko, B.N. Semenov[1,2,3] and Ya.A. Sevastyanov[1,2]

[1]Peter the Great St. Petersburg Polytechnic University,
St. Petersburg 195251, Russia
[2]St. Petersburg State University, St. Petersburg 199034, Russia
[3]Institute of Problems of Mechanical Engineering, Russian Academy
of Sciences, St. Petersburg 199178, Russia

Received: November 23, 2016

Abstract. Deformation and fracture processes in pre-cracked graphene sheets are examined by molecular dynamics simulations. Thin and thick pre-existent cracks in graphene sheets are considered which are generated through removal of one and two (neighboring) chains of carbon atoms, respectively, from a pristine sheet. Tensile tests of graphene sheets with these cracks oriented along zigzag directions were performed. Crack evolution/growth processes were observed and described. Also, for each graphene sheet tested, we revealed stress-strain dependence, maximum elastic strain, maximum plastic strain, and tensile strength.

1. INTRODUCTION

Graphene – a new 2D carbon material – exhibits the excellent electronic, energy-storage, thermal and mechanical properties; see, e.g., reviews [1-10]. For example, in the experiment [11], it was shown that pristine micron-sized graphene is characterized by superior intrinsic strength of ≈ 130 GPa, maximum elastic strain of 25% and huge Young modulus of ≈ 1.0 TPa. These remarkable characteristics are of crucial interest for structural applications of graphene. In addition, lifetime of graphene-based NEMS, nanoelectronic devices and sensors is critically sensitive to the mechanical properties of graphene. Note that real free-standing graphene sheets and graphene layers deposited on substrates often contain defects like line grain boundaries, point defects and cracks. Such defects can appear in graphene during its fabrication and/or exploitation. The presence of defects in graphene is capable of dramatically affecting its mechanical properties; see, e.g., [12-37]. In examinations of the effects of defects on deformation and fracture processes in graphene, many research efforts were focused on the effects exerted by grain boundaries and point defects; see, e.g., [12-29]. Besides, the mechanical properties of pre-cracked graphene structures were examined [30-36]. In doing so, the main attention has been devoted to sensitivity of their mechanical characteristics to crack length, crack orientation and temperature. At the same time, in conventional 3D solids containing pre-existent cracks, ductility, fracture strength and toughness significantly depends on crack thickness at its tip [38-41]. For instance, high ductility and fracture toughness are inherent to coarse-grained polycrystalline metals where crack tips are effectively blunted so that crack

Corresponding author: B.N. Semenov, e-mail: semenov@bs1892.spb.edu

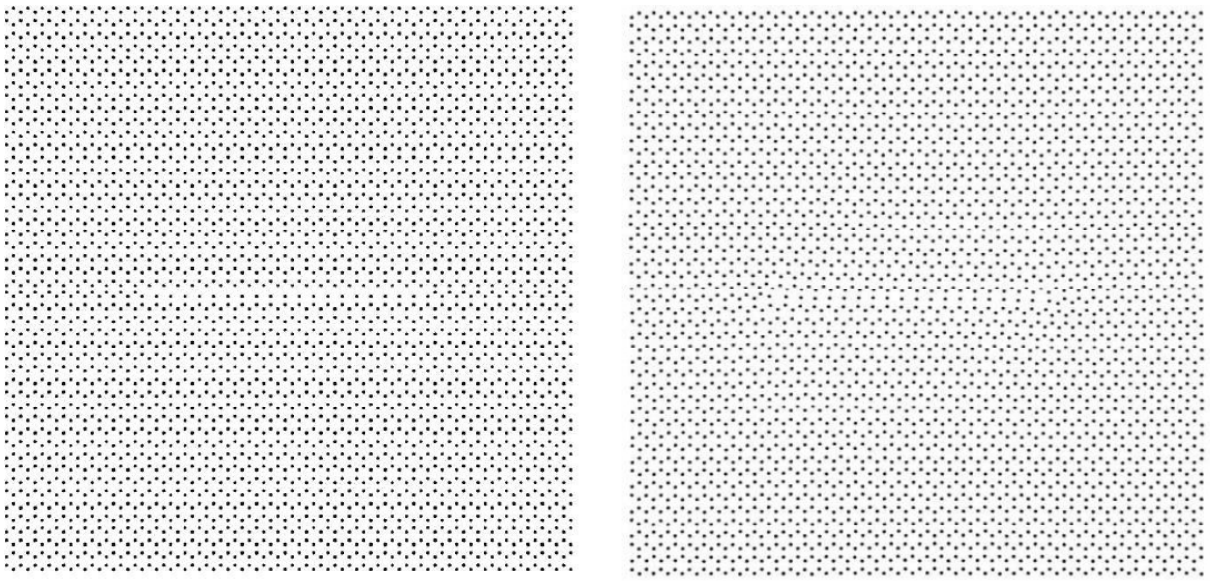

a) b)

Fig. 1. Graphene sheet containing a thin crack. (a) Initial configuration. (b) Configuration after relaxation.

growth is effectively hindered [38, 39]. In contrast, cracks are typically sharp and thereby rapidly grow in nanocrystalline metals [40, 41] which conventionally demonstrate low tensile ductility [42 - 44]. In the context discussed, it is highly interesting to understand the role of crack thickness in crack growth processes in graphene. The main aim of this paper is to examine by molecular dynamics (MD) simulations both deformation and crack growth processes in pre-cracked graphene sheets with a special attention being paid to the effects of crack thickness and chirality on the mechanical characteristics (stress-strain dependence, elastic limit, strain-to-failure and tensile strength) exhibited by these free-standing sheets.

2. SIMULATION METHOD

In description of deformation and fracture processes in pre-cracked graphene sheets, we used the Large-scale Atomic/Molecular Massively Parallel Simulator MD simulation package. In order to specify interatomic bonds, the adaptive intermolecular reactive bond order (AIREBO) potential [45] is utilized. The initial simulation cell has a square-like shape with sizes 10 nm x 10 nm and is characterized by periodic boundary conditions along directions parallel to its edges. The distance between carbon atoms in graphene in its initial state is taken as 1.42 Å.

At the first stage of the pre-simulation procedure, we created two graphene sheets each containing a crack that has length of around 5 nm and is located in the central area of the sheet. The cracks are parallel to the crystallographic zigzag direction of graphene hexagonal lattice (Figs. 1a and 2a), and they are created by removal of i monatomic chains of carbon atoms from a pristine graphene sheet, where i = 1, 2.

At the second stage of the pre-simulation procedure, the initial pre-cracked graphene sheets were relaxed through simulations involving 1,000,000 iteration steps in Nose-Hoover thermostat at room temperature (300 K). As a result of the relaxation procedure, the this crack specified by i = 1 transforms into a chain of 8-disclinations (8-membered rings of carbon atoms) terminated by 5-disclinations (5-membered rings of carbon atoms) (Fig. 1b). That is, due to the relaxation, interatomic bonds between atoms belonging to opposite sides of the crack are enhanced. The thick crack specified by i = 2 slightly expands, that is, distances between atoms belonging to opposite sides of the crack slightly increase (Fig. 2b).

Then the tensile strain was applied to a graphene sheet along the crystallographic armchair direction

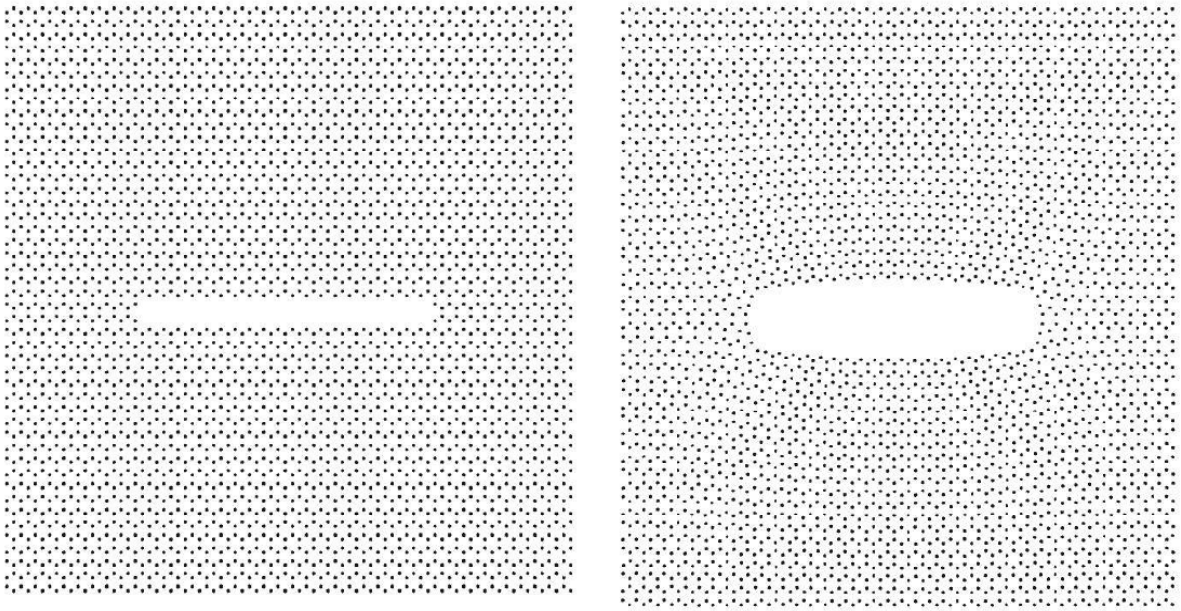

a) b)

Fig. 2. Graphene sheet containing a thick crack. (a) Initial configuration. (b) Configuration after relaxation.

perpendicular to crack line with a strain rate of 0.001 ps^{-1}. Evolution of the pre-cracked graphene structures under tensile deformation will be considered in detail in next section.

3. DEFORMATION AND FRACTURE PROCESSES IN PRE-CRACKED GRAPHENE SHEETS

Following our simulations, evolution of the graphene sheet containing the thin crack under tension occurs as follows. When the tensile load is applied to the graphene sheet, it is elastically strained at a rather extended stage. Then, a very short fracture stage occurs. First, several voids are generated at the site of the pre-existent thin crack (Fig. 3a). In doing so, the damaged region as by practice the same length as the pre-existent crack. The voids under discussion rapidly grow and converge forming one large void (Fig. 3b). Very fast growth of the large void results in complete failure of the graphene sheet, that is, its separation into two isolated pieces.

We now consider deformation and fracture processes occurring in the graphene sheet containing the thick crack under tension. In this case, the elastic deformation stage is by practice absent. When the tensile load is applied to the pre-cracked graphene sheet, the thick crack increases its length through elementary events of plastic deformation and fracture in the vicinity of its tip (in the area where external stress concentration effectively comes into play) (Fig. 4a). Elementary events of plastic deformation in graphene are rearrangements of interatomic C-C bonds. They typically lead to the formation of *n*-disclinations (*n*-membered rings of carbon atoms), where $n = 3, 4, 5$ and 7. Elementary events of fracture are breaks of interatomic C-C bonds. Such events typically result in the formation of crack/void-like *n*-cells, that is, *n*-membered rings of carbon atoms, where $n > 7$ (for details, see a discussion in Ref. [46]).

The plastic deformation stage realized via elementary deformation events and accompanied by elementary fracture events continues giving rise to further elongation of the crack (Fig. 4b). Finally, the crack growth results in complete failure of the graphene sheet.

Fig. 5 presents strain-stress dependences characterizing tension of pre-cracked graphene sheets. The strain-stress dependence for the graphene sheet with the thin crack (Fig. 5a) has an extended elastic deformation stage terminated by fracture reflected as an abrupt fall of the stress-strain curve. The strain-stress dependence for the graphene sheet containing the thick crack (Fig. 5b) by practice does not have an elastic deformation stage.

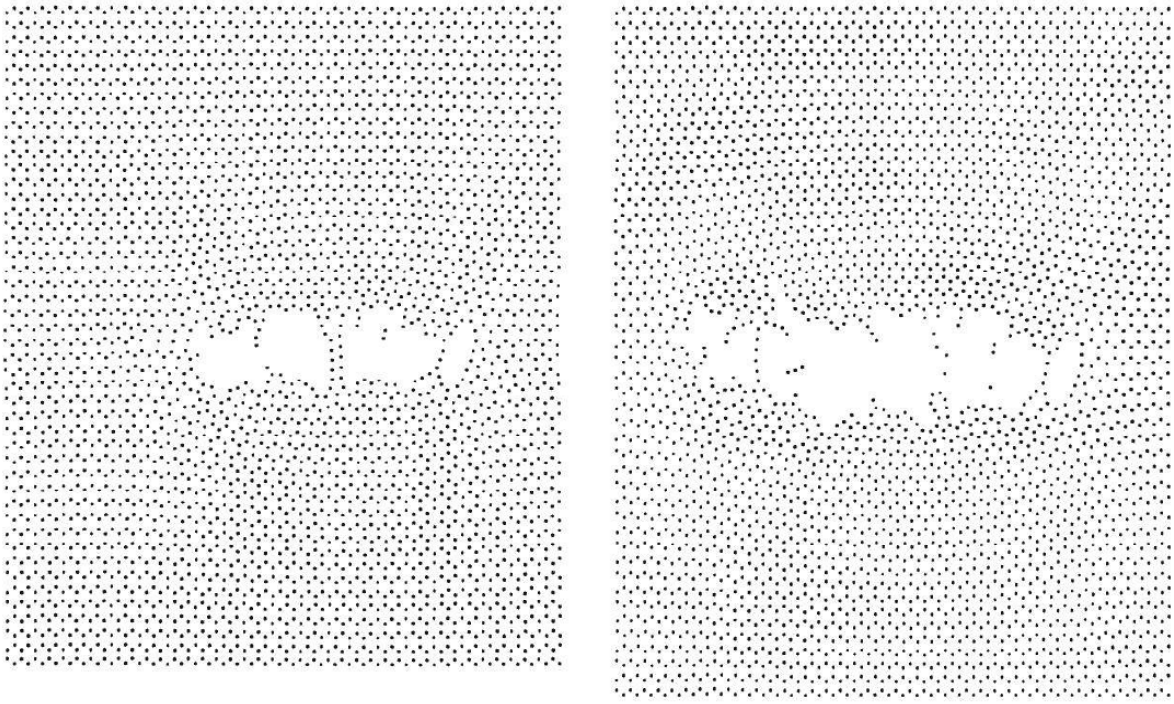

a) b)

Fig. 3. Evolution of mechanically loaded graphene containing a thin crack at (a) the onset of fracture, and (b) the pre-final stage of fracture (for a detailed description, see the main text).

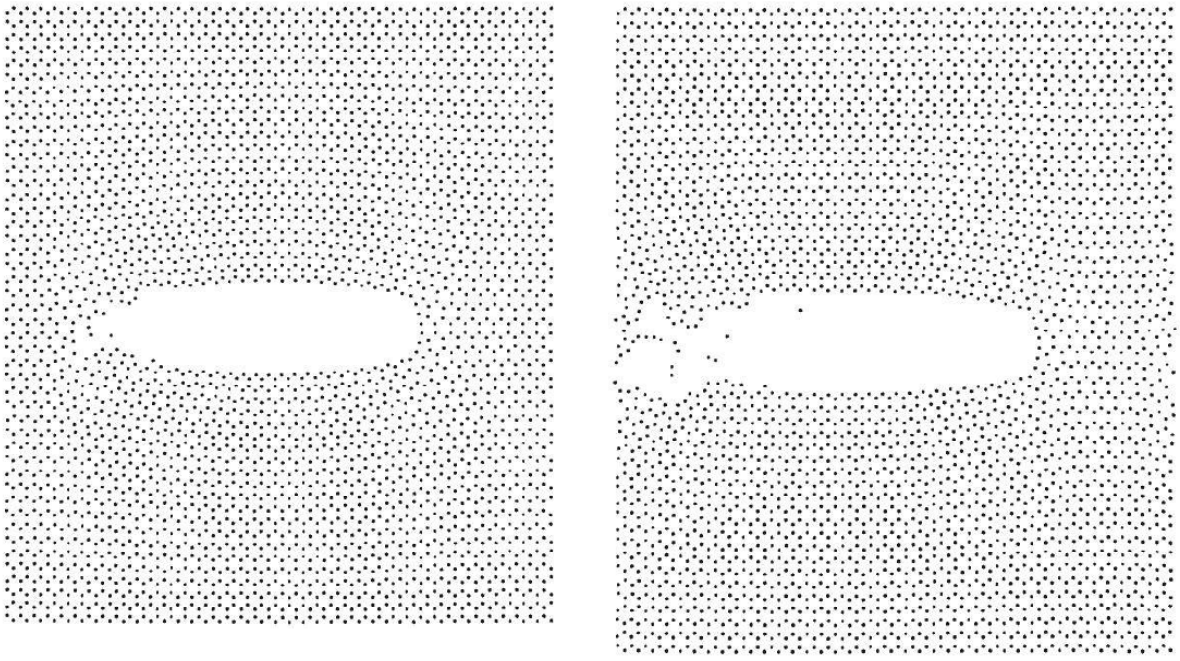

a) b)

Fig. 4. Evolution of mechanically loaded graphene containing a thick crack at (a) the onset of plastic deformation, and (b) the intermediate stage of plastic deformation (for a detailed description, see the main text).

The plastic deformation stage starts to occur at the tension onset. The plastic deformation stage is rather extended and contains many bursts each is associated with either rearrangement or break of an interatomic C-C bond, that is, with either plastic deformation event or fracture event, respectively. The plastic deformation stage is terminated by fracture reflected as an abrupt fall of the stress-strain curve.

We now consider mechanical characteristics (derived from strain-stress dependences in Fig. 5)

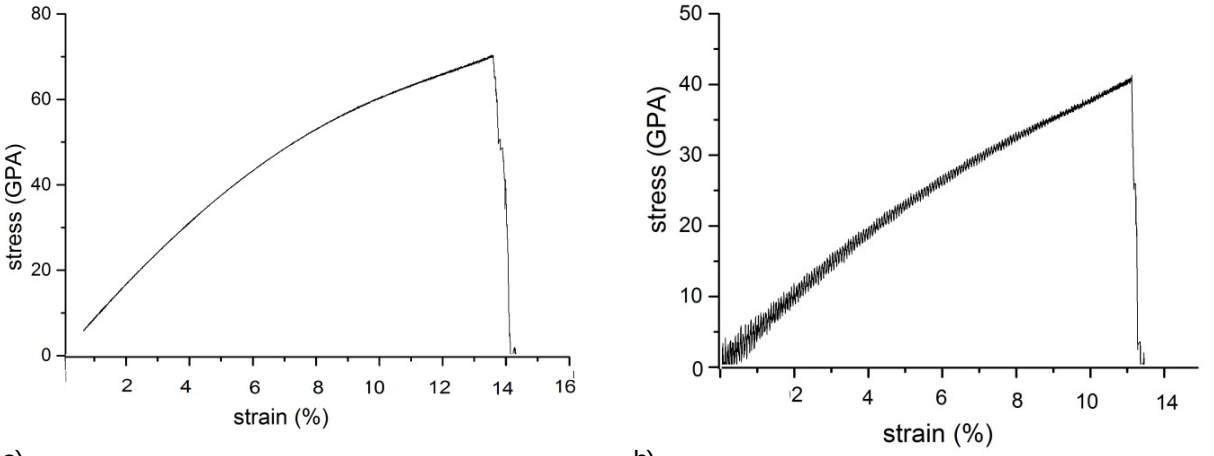

Fig. 5. Strain-stress dependences that characterize deformation and fracture processes in graphene sheets containing thin and thick cracks: (a) and (b), respectively.

of pre-cracked graphene sheets. In the situation with the thin crack, the maximum elastic strain $\varepsilon_{el} \approx 14\%$, the plastic strain $\varepsilon_{pl} \approx 0\%$, and the tensile strength $\sigma_t \approx 70$ GPa. In the situation with the thick crack, the elastic strain $\varepsilon_{el} \approx 0\%$, the maximum plastic strain $\varepsilon_{pl} \approx 11\%$, and the tensile strength $\sigma_t \approx 42$ GPa.

Thus, the graphene sheet initially containing the thin crack exhibits the brittle behavior with the extended elastic deformation stage terminated by catastrophic fracture. The tensile strength of this pre-cracked graphene specimen has value of $\sigma_t \approx 70$ GPa. The value in question is smaller than the tensile strength ($\sigma_{pr\text{-}armchair} = 100$ GPa; see computer simulations [25]) that specifies pristine graphene in tension along the armchair direction.

The graphene sheet initially containing the thick crack is characterized by the absence of the elastic deformation stage and shows functional plasticity with the maximum plastic strain $\varepsilon_{pl} \approx 11\%$. The tensile strength of the graphene specimen with the pre-existent thick crack has value of $\sigma_t \approx 42$ GPa. This value is smaller than that (70 GPa) of its counterpart in the case of the thin crack and significantly smaller than the tensile strength ($\sigma_{pr\text{-}armchair} = 100$ GPa; see computer simulations [25]) that specifies pristine graphene in tension along the armchair direction.

4. CONCLUDING REMARKS

To summarize, with MD simulations, we have examined deformation and fracture processes in pre-cracked graphene sheets under tensile load. Thin and thick pre-existent cracks in graphene sheets were considered which are generated through removal of one and two (neighboring) chains of carbon atoms, respectively, from a pristine sheet (Figs. 1a and 2b, respectively). Tensile tests of graphene sheets with these cracks oriented along zigzag directions were performed. The graphene sheet initially containing the thin crack shows the brittle behavior with the extended elastic deformation stage terminated by catastrophic fracture. The tensile strength of this pre-cracked graphene specimen has value of $\sigma_t \approx 70$ GPa The graphene sheet initially containing the thick crack is characterized by the absence of the elastic deformation stage and demonstrates functional plasticity with the maximum plastic strain $\varepsilon_{pl} \approx 11\%$.

During the extended plastic deformation stage, the thick crack increases its length through elementary events of plastic deformation and fracture in the vicinity of its tip (Fig. 4a). Elementary events of plastic deformation in graphene are rearrangements of interatomic C-C bonds. Elementary fracture events are breaks of interatomic C-C bonds. The plastic deformation stage realized via elementary deformation events and accompanied by elementary fracture events continues giving rise to further elongation of the crack (Fig. 4b). Finally, the crack growth results in complete failure of the graphene sheet. The tensile strength of the graphene specimen with the pre-existent thick crack has value ($\sigma_t \approx 42$ GPa) which is smaller than that (70 GPa) of its counterpart in the case of the thin crack and significantly

smaller than the tensile strength ($\sigma_{pr\text{-}armchair}$ = 100 GPa) that specifies pristine graphene in tension along the armchair direction. Thus, in the examined cases, the tensile strength of a pre-cracked graphene specimen decreases with rising the crack thickness.

ACKNOWLEDGEMENTS

This work was supported, in part (for A.S.K and I.A.O.), by the Ministry of Education and Science of Russian Federation (Zadanie 9.1964.2014/K) and, in part (for B.N.S. and Y.A.S.), by St. Petersburg State University (research grant 6.38.337.2015). The simulations were performed at Resource Center "Simulation Center of St. Petersburg State University".

REFERENCES

[1] A.H. Castro Neto, F. Guinea, N.M.R. Peres, K.S. Novoselov and A.K. Geim // *Rev. Mod. Phys.* **81** (2009) 109.
[2] A.A. Balandin // *Nature Mater.* **10** (2011) 569.
[3] I.A. Ovid'ko // *Rev. Adv. Mater. Sci.* **30** (2012) 201.
[4] K.S. Novoselov, V.I. Fal2 ko, L. Colombo, P.R. Gellert, M.G. Schwab and K. Kim // *Nature* **490** (2012) 192.
[5] I.A. Ovid'ko // *Rev. Adv. Mater. Sci.* **34** (2013) 1.
[6] O.V. Yazyev and Y.P. Chen // *Nature Nanotechnol.* **9** (2014) 755.
[7] I.A. Ovid'ko // *Rev. Adv. Mater. Sci.* **38** (2014) 190.
[8] C. Daniels, A. Horning, A. Phillips, D.V.P. Massote, L. Liang, Z. Bullard, B.G. Sumpter and V. Meunier // *J. Phys.: Condens. Matter* **27** (2015) 373002.
[9] J.-W. Jiang, B.-S. Wang, J.-S. Wang and H.S. Park // *J. Phys.: Condens. Matter* **27** (2015) 083001.
[10] I.A. Ovid'ko, A.V. Orlov // *Rev. Adv. Mater. Sci.* **40** (2015) 249.
[11] C. Lee, X. Wei, J.W. Kysar, J. Hone. // *Science* **321** (2008) 385.
[12] R. Grantab, V.B. Shenoy, R.S. Ruoff // *Science* **330** (2010) 946.
[13] P.Y. Huang, C.S. Ruiz-Vargas, A. M. van der Zande, W.S. Whitney, M.P. Levendorf, J.W. Kevek, S. Garg, J.S. Alden, C.J. Hustedt, Y. Zhu, J. Park, P.L. McEuen, D.A. Muller // *Nature* **469** (2011) 389.
[14] C.S. Ruiz-Vargas, H.L. Zhuang, P.Y. Huang, A.M. van der Zande, S. Garg, P.L. McEuen, D.A. Miller, R.C. Hennig, J. Park // *Nano Lett*. **11** (2011) 2259.
[15] Y. Wei, J. Wu, H. Yin, X. Shi, R. Yang, M. Dresselhaus // *Nature Mater*. **11** (2012) 759.
[16] T.-H. Liu, C.-W. Pao, C.-C. Chang // *Carbon* **50** (2012) 3465.
[17] Y.I. Jhon, S.-E. Zhu, J.-H. Ahn, M.S. Jhon // *Carbon* **50** (2012) 3708.
[18] J. Zhang, J. Zhao, J. Lu // *ACS Nano* **6** (2012) 2704.
[19] M.C. Wang, C. Yan, L. Ma, N. Hu and M.W. Chen // *Comp. Mater. Sci*. **54** (2012) 236.
[20] I.A. Ovid'ko, A.G. Sheinerman // *J. Phys. D: Appl. Phys.* **46** (2013) 345305.
[21] A. Cao, J. Qu // *Appl. Phys. Lett*. **107** (2013) 071902.
[22] J.A. Baimova, L. Bo, S.V. Dmitriev, K. Zhou and A.A. Nazarov // *Europhys. Lett.* **103** (2013) 46001.
[23] C. Carpenter, D. Maroudas and A. Ramasubramaniam // *App. Phys. Lett.* **103** (2013) 013102.
[24] Z. Song, V.I. Artyukhov, J. Wu, B.I. Yakobson, Z. Xu // *ASC Nano* **9** (2013) 401.
[25] A.S. Kochnev, I.A. Ovid'ko, B.N. Semenov // *Rev. Adv. Mater. Sci.* **37** (2014) 105.
[26] A.S. Kochnev, I.A. Ovid'ko // *Rev. Adv. Mater. Sci.* **43** (2015) 89.
[27] Y. Li, D. Datta, Z. Li // *Carbon* **90** (2015) 234.
[28] A.S. Kochnev, N.F. Morozov, I.A. Ovid'ko, B.N. Semenov // *Doklady Physics.* **61** (2016) 239.
[29] A.S. Kochnev, N.F. Morozov, I.A. Ovid'ko, B.N. Semenov // *Doklady Physics.* **61** (2016) 403.
[30] H. Zao, N.R. Aluru // *J. Appl. Phys.* **108** (2010) 064321.
[31] S.S. Terdalkar, S. Huang, H. Yuan, J.J. Rencis, T. Zhu, S. Zhang // *Chem. Phys. Lett.* **494** (2010) 218.
[32] J. L. Tsai, S. H. Tzeng, and Y. J. Tzou, Int. J. Sol. Structures **47** (2010) 503.
[33] M. Xu, A. Tabarraei, J. Paci, J. Oswald, and T. Belytschko, Int. J. Fracture **173** (2012) 163.
[34] M.-Q. Le, R. C. Batra, Comp. Mater. Sci. **69** (2013) 381.
[35] B. Zhang, G. Yang, H. Xu // *Physica B* **434** (2014) 145.

[36] A. Lohrasebi, M. Amini, M. Neek-Amal // AIP Advances **4** (2014) 057113.
[37] H. Yin, H.J. Qi, F. Fan, T. Zhu, B. Wang, Y. Wei // *Nano Lett.* **15** (2015) 1918.
[38] J.R. Rice, R. Thomson // *Philos. Mag*. **29** (1974) 73.
[39] J.R. Rice // *J. Mech. Phys. Solids* **40** (1992) 239.
[40] I.A. Ovid'ko, A.G. Sheinerman // *Scr. Mater*. **60** (2009) 627.
[41] I.A. Ovid'ko, A.G. Sheinerman // *Acta Mater.* **58** (2010) 5286.
[42] C.C. Koch, I.A. Ovid'ko, S. Seal, S. Veprek, Structural Nanocrystalline Materials: Fundamentals and Applications. Cambridge: Cambridge University Press; 2007.
[43] I.A. Ovid'ko, T.G. Langdon // Rev. Adv. Mater. Sci. **30** (2012) 103.
[44] P. Kumar, M. Kawasaki, T.G. Langdon // *J. Mater. Sci*. **51** (2016) 7.
[45] S.J. Stuart, A.B. Tutein and J.A. Harrison // *J. Chem. Phys.* **112** (2000) 6472.
[46] A.S. Kochnev, I.A. Ovid'ko, B.N. Semenov // *Rev. Adv. Mater. Sci.* **47** (2016) 79.